ACS OMEGA

Open Access

http://pubs.acs.org/journal/acsodf

Article

Adsorptive Separation, Interfacial Configuration, and Mechanism of Dimethyl Carbonate−Methanol Azeotrope onto α-Al_2O_3: Experimental and Molecular Simulations

Xueni Sun,* Qiang Fu, Lidong Li, Chunxiang Huang, Jun Wang, and Hui Shao

Cite This: *ACS Omega* 2025, 10, 4026−4036

Read Online

ACCESS | Metrics & More | Article Recommendations

ABSTRACT: Experiments and molecular simulations were combined to investigate the adsorption mechanism of dimethyl carbonate (DMC) and methanol (MeOH) azeotrope onto α-Al_2O_3 while the differences and similarities between pure and azeotropic components were discussed. Static experimental results have shown that α-Al_2O_3 exhibited capacities in an unexpected order as azeotropic MeOH > pure DMC > pure MeOH > azeotropic DMC. MeOH-DMC and pure MeOH both fitted the PFO model with proximal kinetic constants, while the pure DMC exhibited a different behavior with a diffusion-controlled stage followed by chemisorption. The interfacial configuration as well as the mechanism at the molecular level was studied by molecular dynamics and density functional theory. Molecular simulation results indicate that a multilayer adsorption conformation is formed on the α-Al_2O_3 (0 0 1) surface for MeOH-DMC with most Al sites being occupied by MeOH followed by DMC constructing a bilayerlike structure with the preadsorbed MeOH molecules. Moreover, the adsorption of DMC can further reduce the dissociation of preadsorbed MeOH. This factor seems to promote the adsorption of more MeOH molecules on the α-Al_2O_3 (0 0 1) surface, leading to DMC aggregation outside the MeOH layer.

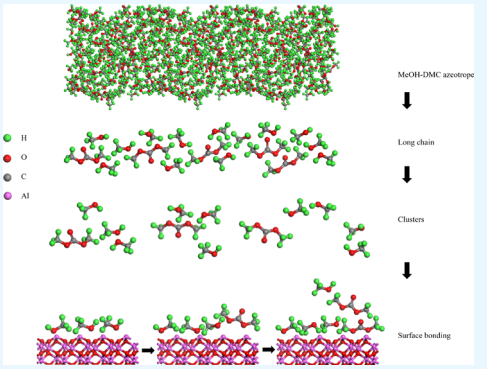

1. INTRODUCTION

Dimethyl carbonate (DMC) is a green chemical raw material with low toxicity and high biodegradability.[1] DMC (CH_3O−CO-OCH_3) contains carbonyl, methyl, and methoxy carbonyl groups, which can be applied to replace hazardous reagents such as phosgene and dimethyl sulfate to produce various high-value products.[2] Moreover, given its high octane number (105), high oxygen content (53.28%), and high H/C ratio, DMC has been also employed as an ideal fuel additive that reduces particle matter and soot emission.[3,4] In addition, there is a rapid development of DMC being used as a solvent especially in the electronics industry due to its good solubility and high dielectric constant.[5] Concerning the widespread applications of DMC, the global production of DMC is expected to exceed 300 kilotons by the end of 2025 while the DMC demand will rise to about 450−1600 kilotons/a.[6,7] DMC can be synthesized via several methods including transesterification, oxidative carbonylation, urea alcoholysis, direct synthesis from CO_2, and so on.[8] However, most of these synthesis processes use excessive methanol (MeOH) as the feedstock to guarantee the product yield.[9] Therefore, the production of high-quality DMC always faces the problem of separating the MeOH-DMC azeotrope.

At present, the main techniques for the separation of MeOH-DMC azeotrope include pressure swing distillation (PSD), extractive distillation (ED), membrane separation, and adsorption.[10−13] Currently, PSA is an effective but energy-intensive method for the separation of homogeneous azeotropes with a high operating cost and equipment investment issues.[14,15] ED has been considered more economical than PSD.[16,17] However, toxic solvents may cause environmental problems. Membrane separation, especially pervaporation (PV), has received widespread attention.[18] However, this technique faces challenges of low processing capacity and short membrane life.[19] Compared with other techniques, adsorption demonstrates several advantages including its mild condition, simple operation, and low energy consumption which has been considered as one of the most promising separation methods.[20] Apparently, adsorbents are always crucial for the adsorption process, and various adsorbents have been studied for the separation of MeOH-DMC azeotrope. Hydrophilicity or hydrophobicity is an important factor in the separation of MeOH-DMC given

Received: November 3, 2024
Revised: January 1, 2025
Accepted: January 9, 2025
Published: January 21, 2025

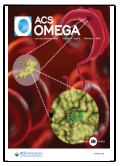

that MeOH contains a hydroxyl group (−OH). Micheal Spencer conducted the adsorption process in a packed bed loading with silicalite (Si/Al > 20) as the adsorbent with less than 50% of the DMC being taken up by the silicalite.[21] Later, Fan et al.[22] increased the removal ratio of DMC to 86% by applying silicate-1 (Si/Al > 360) as the adsorbent. Although the hydrophobicity was improved, the adsorption capacity did not significantly increase, only 34.8 mg/g. The pore size is also a prominent factor in the adsorption separation because of the difference in molecular diameters of MeOH and DMC.[23] Accordingly, five supporting materials with different surface areas and pore sizes have been applied in MeOH-DMC separation, including WAPO-5, ZSM-22, TS-1, H-beta, and palygorskite (Pal).[24] However, static adsorption studies have shown that the physical structures of the adsorbents do not significantly affect their separation performance. In addition to the properties mentioned above, interactions between adsorbates and active sites are also essential. Sun et al.[25] tried to adsorb MeOH from the azeotrope by impregnating Al_2O_3 onto attapulgite (ATP) because the hydroxyl O atom of MeOH can form a chemical bond with Al sites. The synthesized CTAB/Al_2O_3/ATP adsorbent showed a high capacity toward MeOH of 217.56 mg/g with a separation selectivity equaling 7.63. They further increased the adsorption capacity of MeOH to 621.62 mg/g while maintaining the separation selectivity by loading Al_2O_3 onto palygorskite (Pal).[24] Based on the static experimental results, Al_2O_3 has shown the highest MeOH uptake and demonstrated a promising separation performance among many metal oxides. Therefore, Al_2O_3 as a common adsorbent plays an important role in MeOH-DMC separation.

Among different kinds of Al_2O_3, α-Al_2O_3 shows low activity, extreme hardness, and high stability when compared with porous γ-Al_2O_3.[26] As a result, α-Al_2O_3 is a good metal matrix composite reinforced phase while γ-Al_2O_3 is often used as an adsorbent.[27,28] Due to the large surface area and high porosity, γ-Al_2O_3 should have a higher adsorption capacity. However, previous research results indicated that both α-Al_2O_3 and γ-Al_2O_3 have shown similar adsorption capacity for MeOH around 320 mg/g.[29] However, α-Al_2O_3 was more effective in the separation of MeOH-DMC because it had a lower DMC uptake when compared with γ-Al_2O_3. Hence, the adsorption of the MeOH-DMC azeotrope onto α-Al_2O_3 and the difference between pure and azeotropic components have attracted our research interest. Furthermore, both the characteristics of the adsorbate and solid materials should be taken into consideration when exploring the adsorption mechanism. It is not hard to tell that MeOH-DMC azeotrope has its unique property which cannot be simply represented by pure MeOH or DMC. As a result, the difference or similarity between the pure and azeotropic components is an issue worth exploring.

In this study, adsorption experiments, kinetic modeling, molecular dynamics (MD), and density functional theory (DFT) were combined to investigate the difference between pure solution and azeotropic mixture as well as to reveal the corresponding adsorption mechanism. Initially, batch experiments were carried out to obtain the adsorption capacities of MeOH and DMC using pure solutions and azeotrope mixture, in which α-Al_2O_3 was applied as the adsorbent. Subsequently, adsorption kinetics were simulated by two mathematical models to provide information on mass transfer behaviors. Then, the adsorption conformations and spacious distribution of molecules on the α-Al_2O_3 surface were clarified by adsorption energy, relative concentration, and radial distribution functions (RDFs). Lastly, the formation of bonds and charge transfer at the surface preadsorbed with adsorbates were explored at a molecular level by DFT calculations. This work aims to provide more useful information on the adsorptive separation of MeOH-DMC azeotrope.

2. EXPERIMENTAL SECTION

2.1. Experimental Details. *2.1.1. Materials.* α-Al_2O_3 adsorbents were obtained from Aladdin Scientific Corp. MeOH, DMC, and m-xylene were all purchased from Sinopharm Chemical Reagent Co., Ltd. *N*,*N*-dimethylformamide (*N*,*N*-DMF) as an inert solvent was purchased from Chinasum Specialty Products Co., Ltd. All chemical reagents were of analytical grade and used without further purification.

2.1.2. Batch Experiments. The procedure of adsorbent preparation and the batch adsorption experiments carried out in this study are the same as those in the previous study.[24,25] During the batch experiment, liquid samples were collected at regular time intervals and analyzed by gas chromatography with a flame ionization detector (GC-FID). The adsorption capacity at time t and the equilibrium adsorption capacity were then calculated using the following formula:

$$q_t = (C_0 - C_t) \times m_L/m_S \quad (1)$$

$$Q = (C_0 - C_e) \times m_L/m_S \quad (2)$$

where q_t (mg/g) is the adsorption capacity at time t, Q (mg/g) is the equilibrium adsorption capacity, C_0 (wt %) is the initial concentration of MeOH or DMC in the liquid, C_t (wt %) is the remaining concentration of MeOH or DMC in the liquid at time t, C_e (wt %) is the equilibrium concentration of MeOH or DMC in the liquid, m_L (g) is the weight of the liquid, and m_S (g) is the weight of the solid adsorbent.

After reaching the equilibrium status, the selectivity S can be determined using the following equation:

$$S = Q_{MeOH}/Q_{DMC} \quad (3)$$

where Q_{MeOH} (mg/g) is the equilibrium adsorption capacity of MeOH, and Q_{DMC} (mg/g) is the equilibrium adsorption capacity of DMC.

The adsorption capacities for pure MeOH and DMC were also investigated for reference with the same method and compared with those results obtained for the azeotrope. The MeOH-DMC azeotrope solution contained 35 wt % MeOH, 15 wt % DMC, and 50 wt % DMF. In order to maintain the same concentration of the corresponding component in the azeotrope, pure MeOH solutions were prepared at a ratio of 35 wt % MeOH and 65 wt % DMF while the concentration of DMC in pure solution was kept at 15 wt % by mixing with 85 wt % DMF.

2.1.3. Sample Analysis. The quantitative analysis of MeOH, DMC, and N, N-DMF in liquid samples was conducted by GC-FID, using m-xylene as an internal standard. The initial column temperature was at 70 °C and kept at that temperature for 1 min. Then the column temperature increased to 150 °C at 35 °C/min and remained there for 1 min. The injection temperature was maintained at 200 °C. To reduce errors, each sample was analyzed three times under the same conditions, and the average value was calculated.

2.2. Computational Details. All of the computational simulations were completed using Materials Studio (MS)

https://doi.org/10.1021/acsomega.4c10016
ACS Omega 2025, 10, 4026−4036

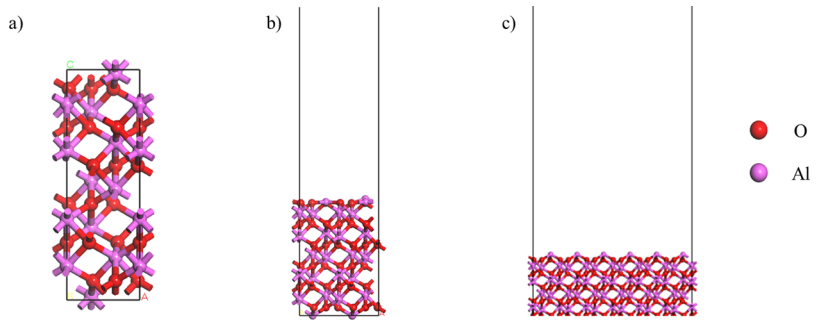

Figure 1. Optimized configurations of (a) α-Al_2O_3 (0 0 1) cell, (b) (2 × 2 × 1) supercell, and (c) (4 × 2 × 1) supercell.

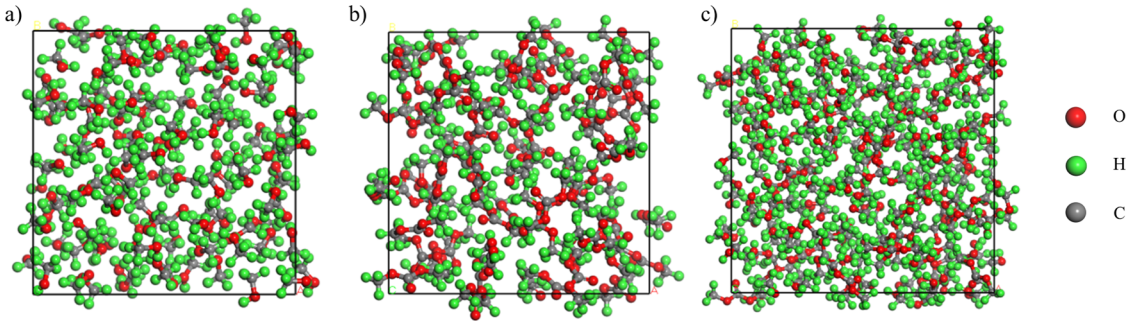

Figure 2. Simulation solution boxes of (a) pure MeOH, (b) pure DMC, and (c) azeotropic MeOH-DMC.

software. The geometric structures of α-Al_2O_3, MeOH, and DMC were optimized through the DFT method conducted in the Dmol^3 module. The Perdew−Burke−Ernzerhof (PBE) generalized gradient approximation (GGA) with a double numerical quality set (DNP) was chosen to describe the electron change and exchange-correlation interactions. The DFT-D method of Grimme was selected to describe van der Waals interactions. The energy convergence tolerance was set to 1.0×10^{-5} Ha with a maximum force of 0.002 Ha/Å while the maximum displacement for the convergence criteria was 0.005 Å. The Monkhorst−Pack scheme k-point mesh grid was set to 3 × 3 × 1.

The α-Al_2O_3 (0 0 1) surface has been proven to be the most stable surface with the lowest energy.[30] Therefore, α-Al_2O_3 (0 0 1) was chosen for the surface construction in this study. The lattice parameters of α-Al_2O_3 (0 0 1) were: $a = b = 4.759$ Å, $c = 12.991$ Å, $\alpha = \beta = 90°$, $\gamma = 120°$, which were in good agreement with values from previous studies.[31] A (2 × 2 × 1) supercell and a (4 × 2 × 1) supercell with a vacuum layer were constructed for α-Al_2O_3 (0 0 1) for DFT and MD calculations, respectively. The vacuum layer was set to 40 Å to eliminate the interactions between crystal surfaces caused by the periodic boundary condition on the system. The smart algorithm with a convergence level of 0.001 kcal/mol was used for the optimization of the crystal geometry. The structures of MeOH and DMC were also optimized by using the same convergence criteria and calculation parameters. Figure 1 shows the optimized configuration of α-Al_2O_3 (0 0 1) cells and supercells.

The adsorption of pure MeOH, pure DMC, and MeOH-DMC solutions on α-Al_2O_3 (0 0 1) was explored through the molecular dynamic simulation. First, the pure and azeotropic solution boxes were built in the Materials Visualizer module and Amorphous Cell module. The pure MeOH solution box contained 120 molecules, while the pure DMC solution box contained 60 molecules. The density values were set to 0.791 g/cm^3 and 1.07 g/cm^3 for MeOH and DMC, respectively[32,33]. The azeotropic solution box containing 180 MeOH molecules and 30 DMC molecules were then constructed with the density being set to 0.84 g/cm^3 based on the experimental data.[34] The optimized configurations of the simulated solution boxes are displayed in Figure 2.

A layer adsorption model was constructed by placing the solution box on the optimized alumina surface by using the Build Layers module. A COMPASS II force field was selected for this adsorption system. Atom-based summation and Ewald summation were adopted for the calculation of the van der Waals force and electrostatic energy. The energy was minimized using a convergence criterion of 0.5 kcal/(mol Å). The cutoff distance was set to 12 Å. The simulation was run for 2000 ps at 298 K in NVT ensembles implemented at the Nose thermostat using a time step of 1 fs. The initial adsorption models before MD simulations are illustrated in Figure 3.

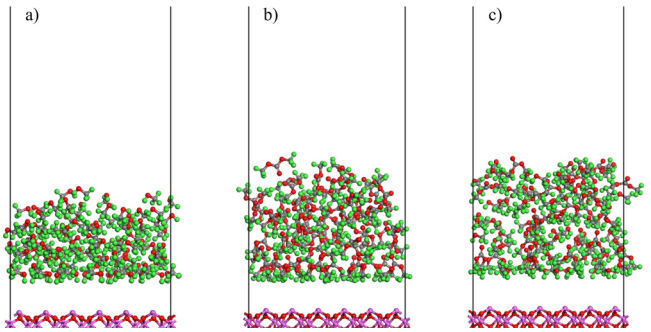

Figure 3. Initial layer configurations of (a) pure MeOH, (b) pure DMC, and (c) MeOH-DMC adsorbed on α-Al_2O_3 (0 0 1).

https://doi.org/10.1021/acsomega.4c10016
ACS Omega 2025, 10, 4026−4036

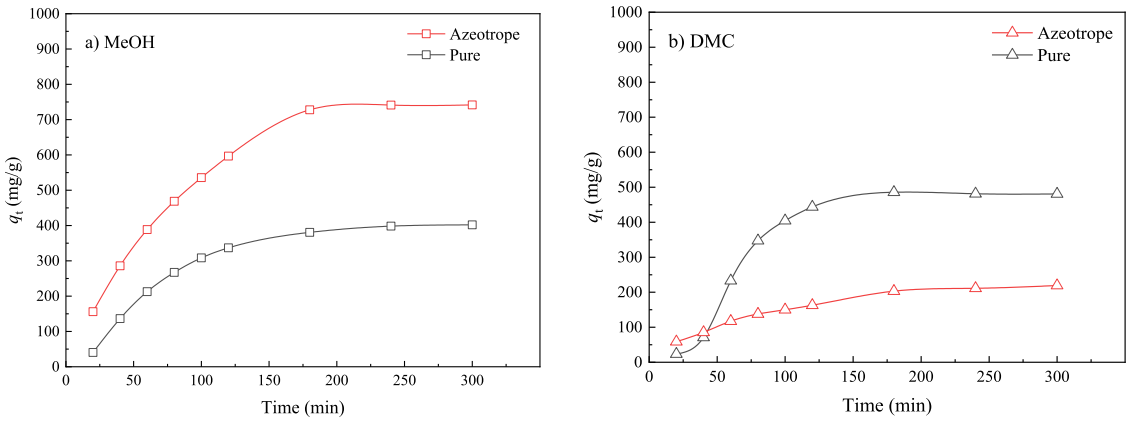

Figure 4. Static adsorption capacities for (a) MeOH and (b) DMC of the pure solution and azeotropic mixture.

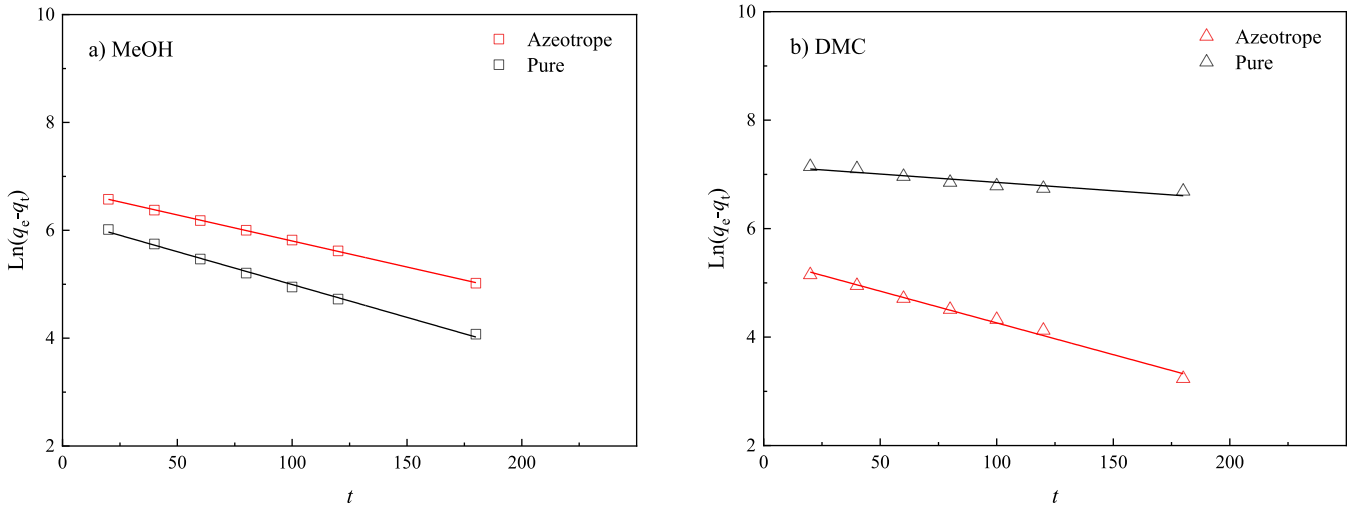

Figure 5. PFO fittings for (a) MeOH and (b) DMC of the pure solution and azeotropic mixture.

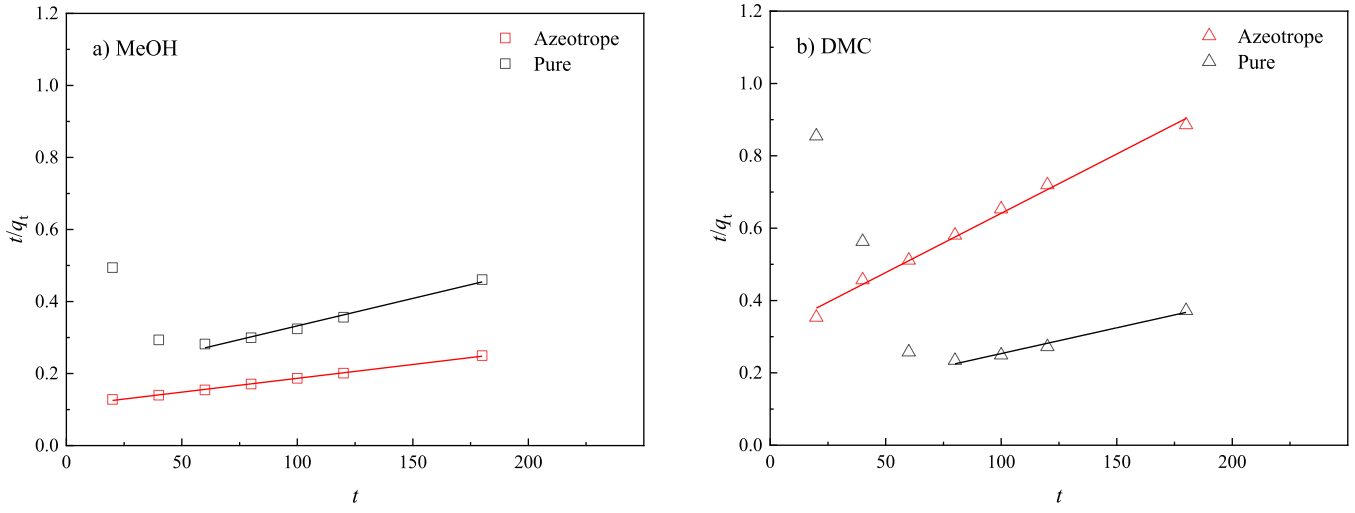

Figure 6. PSO fittings for (a) MeOH and (b) DMC of the pure solution and azeotropic mixture.

3. RESULTS AND DISCUSSION

3.1. Static Experimental Results. The static experiments were carried out using pure solutions and an azeotrope mixture under ambient conditions. The adsorption curves by plotting adsorption capacity q against time t are shown in Figure 4. The adsorption equilibria were all observed at around 180 min. For the adsorption of MeOH-DMC azeotrope by α-Al_2O_3, the adsorption capacity of azeotropic MeOH was much higher than that of azeotropic DMC. The final equilibrium capacities of MeOH and DMC in the azeotrope were 741.24 and 211.36 mg/g, separately. As a result, the selectivity S toward MeOH of α-Al_2O_3 was 3.51. Therefore, α-Al_2O_3 exhibited a promising

https://doi.org/10.1021/acsomega.4c10016
ACS Omega 2025, 10, 4026−4036

Table 1. Adsorption Kinetic Parameters of MeOH and DMC onto α-Al_2O_3

		MeOH		DMC	
		pure	azeotrope	pure	azeotrope
	q_{exp} (mg/g)	398.41	741.24	481.40	211.36
PFO	q_e (mg/g)	497.70	871.31	1286.91	228.61
	k_1 (1/min)	0.0122	0.0097	0.0031	0.0117
	R^2	0.9963	0.9996	0.8726	0.9907
PSO	q_e (mg/g)	653.59	1302.00	704.23	304.88
	$k_2 \times 10^5$ (g/mg/min)	1.3022	0.5360	1.8149	3.4321
	R^2	0.9865	0.9985	0.9807	0.9923

separation performance toward MeOH-DMC azeotrope, which is consistent with our previous study.[29] However, for the adsorption of pure substances, that is not the case. The final amount of pure DMC adsorbed by α-Al_2O_3 was 481.40 mg/g, while the saturated capacity of pure MeOH was only 398.41 mg/g. Moreover, when judging from the two curves in Figure 4a, α-Al_2O_3 adsorbed more MeOH from the azeotrope than from the pure solution. It seems that in the presence of DMC, more MeOH molecules will be attracted to the active sites. Meanwhile, due to the large number of active sites occupied by MeOH, the adsorption capacity of DMC in the azeotrope decreased significantly, as shown in Figure 4b. Not only the capacity but also the mass transfer rate of DMC was significantly slowed down by MeOH molecules appearing in the azeotrope when comparing the slopes of two curves in Figure 4b.

3.2. Adsorption Kinetics. To gain a deeper understanding of the adsorption system, the static experimental data were linearly fitted to two kinetic models, namely, the pseudo-first-order (PFO) equation and the pseudo-second-order (PSO) equation, expressed by eqs 4 and 5. Considering the crucial effect of the data selection on model regression, data points after the equilibrium (t > 180 min) should not be used.[30] Thus, data points before and at equilibrium were then applied for linear fitting in this study.

$$\ln(q_e - q_t) = \ln q_e - k_1 t \tag{4}$$

$$t/q_t = 1/k_2 q_e^2 + t/q_t \tag{5}$$

where q_e (mg/g) and q_t (mg/g) are the amounts of MeOH or DMC adsorbed at equilibrium and time t (min), k_1 is the PFO rate constant (1/min), and k_2 (g/mg/min) is the PSO rate constant.

Fitting curves for MeOH-DMC adsorbed by α-Al_2O_3 are shown in Figures 5 and 6, while the related kinetic parameters are summarized in Table 1. For pure MeOH and azeotropic MeOH, the experimental data fitted the PFO equation better based on the obtained correlation coefficient R^2, which suggests that it is a diffusion-controlled process.[35] Each active site on the α-Al_2O_3 surface could only be occupied by one molecule. In addition, no big difference in the rate constant k_1 was observed between pure MeOH and azeotropic MeOH, suggesting that DMC contained in the azeotrope will not affect the transfer rate of MeOH from the bulk liquid to the surface sites. For DMC, the mass transfer behavior became complicated. Based on the fitting results, neither PFO nor PSO can accurately describe the kinetics of pure DMC. However, when dividing the whole adsorption process into two stages, the initial process (t < 60 min) fitted the PFO suggesting that the adsorption of pure DMC is mainly controlled by the film diffusion. After 60 min, it fitted the PSO indicating that the chemisorption is the rate-controlling step.[36] For azeotropic DMC, although PSO had a better determination coefficient (R^2 = 0.9923), the estimated value of q_e was 304.88 mg/g, which was far from the experimental result. As a result, we have considered that PFO is more suitable than PSO to describe the kinetics for adsorption of azeotropic DMC. Obviously, there are differences in kinetics when compared to pure DMC with azeotropic DMC. Thus, the MeOH contained in the azeotrope might not only affect the adsorbed amount of DMC but also the adsorption mechanism. As a result, MeOH-DMC and pure MeOH both fitted the PFO model with similar kinetic constants while the mass transfer of pure DMC was complex with two stages. The possible explanation is that MeOH-DMC contains abundant long chain structures of $(MeOH)_n$ and DMC-$(MeOH)_m$, which is highly similar to the liquid-phase structure of pure MeOH.[37] Therefore, MeOH-DMC and pure MeOH exhibit a consistent mass transfer behavior in the bulk liquid phase.

3.3. MD Simulations. The MD simulation studies of pure MeOH, pure DMC, and MeOH-DMC adsorbed on α-Al_2O_3 (0 0 1) were carried out to reveal the possible mechanism at the molecular level, including the adsorption energy, diffusivity, equilibrium configurations, relative concentration, and RDF.

The adsorption energy E_{ads} is one of the main parameters to characterize the binding strength between the adsorbate and adsorbent which can be used to analyze the interaction between molecules and the α-Al_2O_3 (0 0 1) surface. For the MD simulation of MeOH-DMC adsorbed onto α-Al_2O_3 (0 0 1), the E_{ads}(kJ/mol) was calculated by eq 6.[38]

$$E_{ads} = E_{total} - E_{substrate} - E_A \tag{6}$$

where E_{total} (kJ/mol) represents the total energy of the system after the molecule adsorbs on the adsorbent surface, $E_{substrate}$ (kJ/mol) represents the energy of the adsorbent, and E_A (kJ/mol) represents the energy of adsorbate A.

The computed E_{ads} results are listed in Table 2. Apparently, the pure substances and azeotropic molecules can be adsorbed onto the α-Al_2O_3 (0 0 1) surface because all calculated adsorption energies were negative.[39] The affinity between the adsorbate and the surface can be determined based on the

Table 2. Adsorption Energy and Diffusivity of Pure and Azeotropic Solutions Adsorbed on α-Al_2O_3 (0 0 1) Surface

		adsorption energy	
solution	component	E_{ads} (kJ/mol)	diffusivity D (10^{-6} cm^2/s)
pure	MeOH	−188.370	0.78
	DMC	−159.816	2.28
azeotrope	MeOH	−250.997	0.45
	DMC	−133.046	4.81

https://doi.org/10.1021/acsomega.4c10016
ACS Omega 2025, 10, 4026−4036

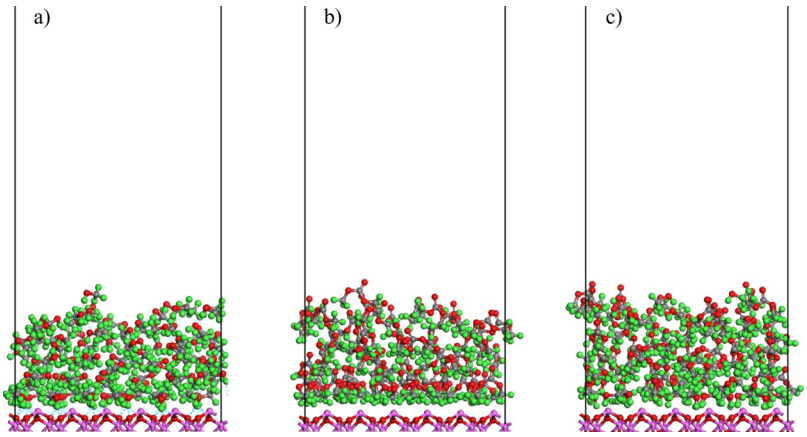

Figure 7. Optimized adsorption configurations of (a) pure MeOH, (b) pure DMC, and (c) azeotropic MeOH-DMC on α-Al_2O_3 (0 0 1).

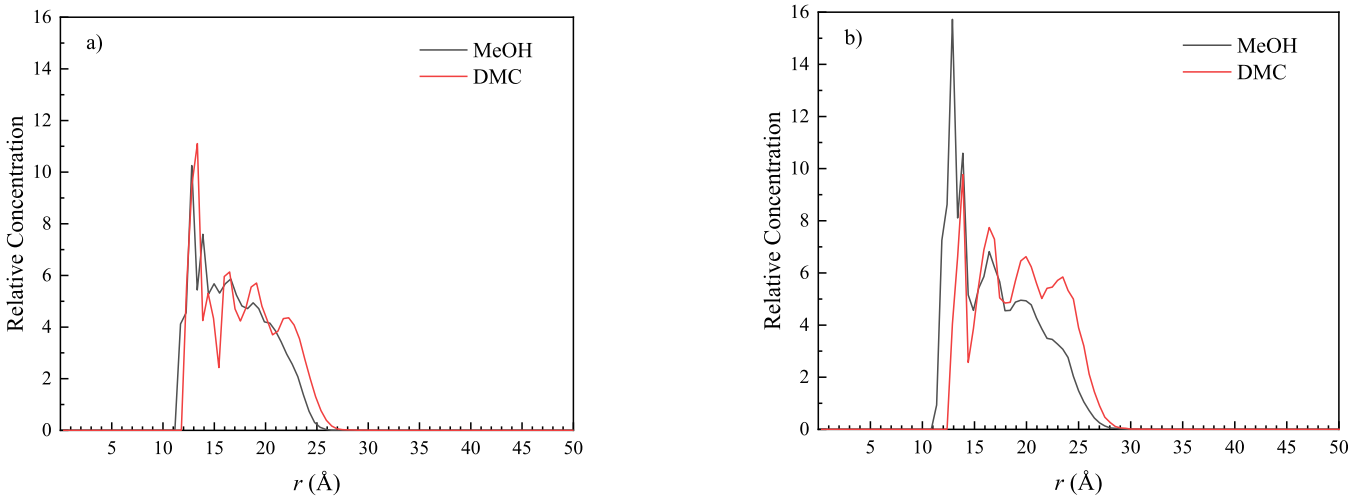

Figure 8. Relative concentration for (a) pure solution and (b) MeOH-DMC.

value of the adsorption energy. As shown in Table 2, E_{ads} of MeOH was much smaller than E_{ads} of DMC for both pure and azeotropic solutions, which indicates that the binding ability of MeOH with the α-Al_2O_3 surface is much stronger than that of DMC. In other words, MeOH is more easily adsorbed onto the α-Al_2O_3 (0 0 1) surface. Moreover, a comparison of E_{ads} between pure MeOH and azeotropic MeOH also suggests that the azeotropic MeOH exhibited a stronger binding strength with surface active sites. However, the interaction between azeotropic DMC with surface active sites weakened, judging from the values of E_{ads} of pure and azeotropic DMC. Based on the E_{ads} results, α-Al_2O_3 demonstrates a promising ability to break the MeOH-DMC azeotrope.

Besides E_{ads}, the diffusivity D (cm^2/s) is another quantity reflecting the interaction strength between the adsorbate and α-Al_2O_3 (0 0 1) surface.[40] The diffusivity represents the average displacement of a particle over a unit area in a unit time, which can be calculated by the following equation.[41]

$$D = 1/6N\left\{\lim_{t\to\infty} d\sum_{i=l}^{N} < \left[r_i\left(t\right) - r_i\left(0\right)\right]^2 > /dt\right\} \quad (7)$$

where D (cm^2/s) is the diffusion coefficient, N is the number of particles, t represents time, r_i (t) (cm) represents the position of particles at time t (s), and r_i (0) (cm) represents the initial position of particles at time t.

Azeotropic MeOH had the smallest value ($D = 0.45 \times 10^{-6}$ cm^2/s) while azeotropic DMC had the highest value ($D = 4.81 \times 10^{-6}$ cm^2/s) among all diffusivities. The larger the value of D, the more easily molecules move on the surface. In that case, the movement of azeotropic MeOH molecules near the surface is completely restricted, which indicates that there exists a very strong interaction between azeotropic MeOH and α-Al_2O_3. Meanwhile, azeotropic DMC had the weakest affinity with the α-Al_2O_3 (0 0 1) surface. This is also consistent with the adsorption energy results.

Aside from the binding strength provided by E_{ads} and diffusivity, the adsorption configuration and the spacious distribution of the molecules on the solid surface are important findings from the MD simulations. After the optimization, the final configurations of pure substances and MeOH-DMC on the α-Al_2O_3 (0 0 1) surface are reflected in Figure 7. Abundant H atoms were attached to the surface O atoms for all three cases while several O atoms in MeOH and MeOH-DMC tended to form O−Al bonds with a solid surface.

Based on the equilibrium configurations, the concentration profiles along the z-axis of the crystal bottom were calculated to analyze the conformations and spacious distribution of molecules. It can be seen from Figure 8 that pure MeOH, pure DMC, azeotropic MeOH, and azeotropic DMC all have sharp

https://doi.org/10.1021/acsomega.4c10016
ACS Omega 2025, 10, 4026−4036

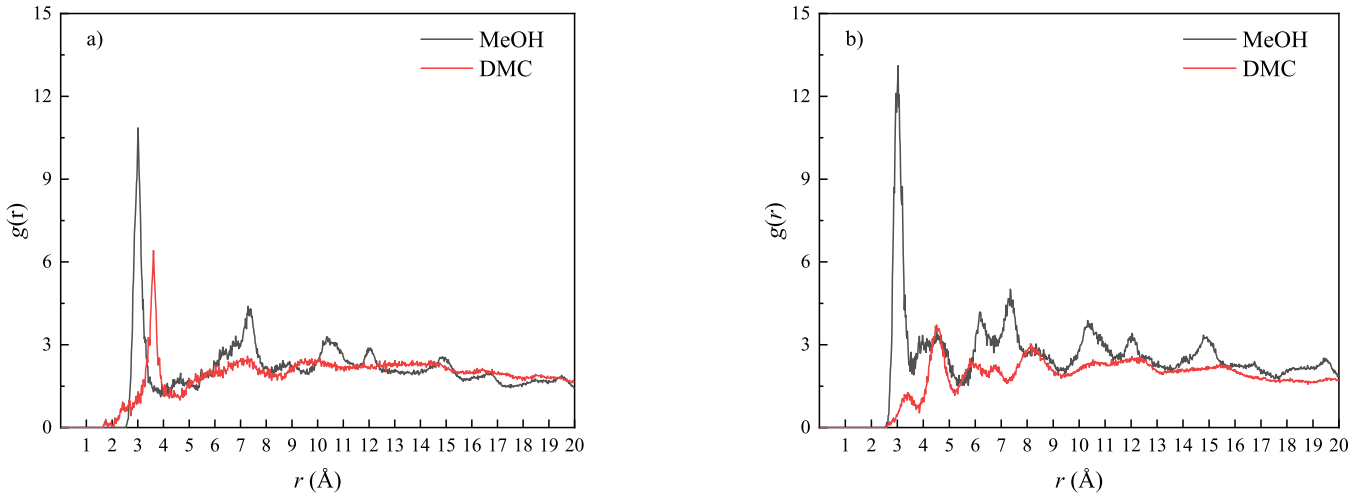

Figure 9. Radial distribution function of MeOH and DMC from (a) pure solution and (b) azeotrope.

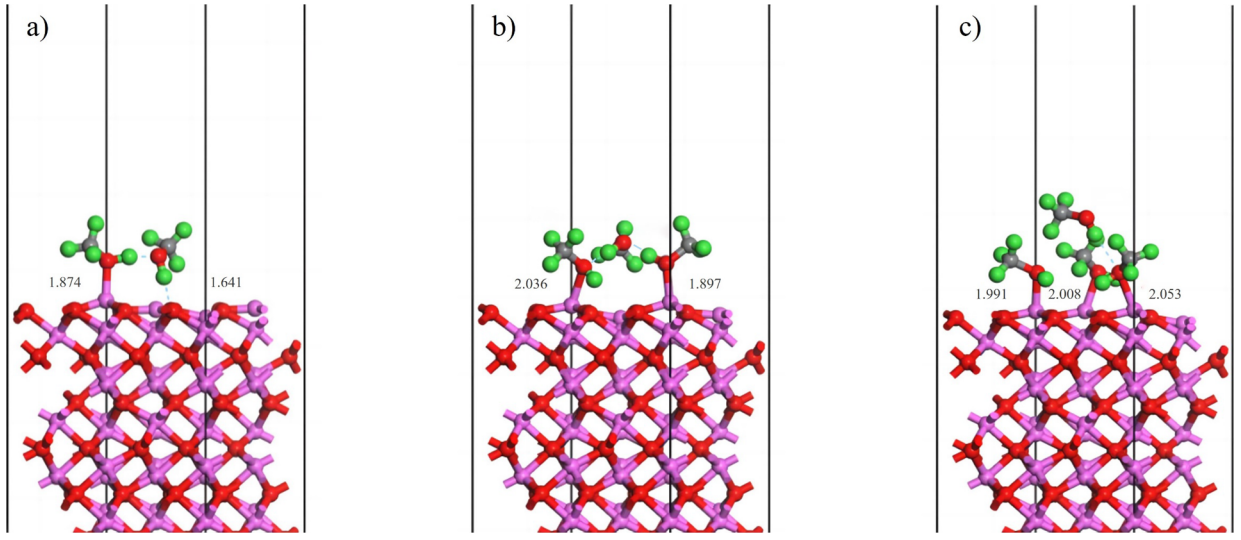

Figure 10. Adsorption of MeOH on the surface preadsorbed with (a) 1 MeOH, (b) 2 MeOH, and (c) 3 MeOH.

peaks at a distance of around 13 Å. It is clear that abundant molecules have adsorbed on the α-Al_2O_3 (0 0 1) surface. The highest peak values of pure MeOH and pure DMC were 10.26 and 11.11, separately, indicating that more DMC molecules have been attracted by the active sites. Meanwhile, multiple peaks were observed for pure DMC at a distance of 15−30 Å while only one broad peak was observed for pure MeOH. Therefore, in addition to monolayer adsorption, the remaining pure MeOH molecules were distributed evenly in space. For azeotropic MeOH and azeotropic DMC, the highest peak values were at 15.72 and 9.77, respectively, indicating that Al_2O_3 has adsorbed more MeOH molecules than DMC from the azeotropic mixture. The order of the highest peak values was azeotropic DMC < pure MeOH < pure DMC < azeotropic MeOH, which is consistent with the experimental results. The distribution of azeotropic DMC and pure substance did not change significantly with multiple peaks being observed. However, the bond distance of the strongest peak shifted away from the surface for azeotropic DMC, which could have been achieved by DMC molecules being stacked on the adsorbed MeOH. Meanwhile, the adsorption conformation of azeotropic MeOH was different from that of pure MeOH, which was close to the profile of DMC with several adsorption layers. In other words, the distribution of azeotropic MeOH is affected by DMC in the MeOH-DMC system. This may be caused by the formation of DMC-$(MeOH)_n$ clusters.[29]

The RDF, also called the pair correlation function, is one of the most useful methods to reveal structural information at molecular length scales.[42] In the MD simulation, the RDF was calculated by the following equation.[43]

$$g(r) = dN/4\pi\rho r^2 dr \quad (8)$$

Within the range of r (Å) to $r + dr$, dN:

$$dN = 4g(r)r^2\rho dr \quad (9)$$

where N is the number of particles, dN is the number of particles between the distance r and $r + dr$, ρ is the density of space, and $g(r)$ refers to the probability that the aluminum atom in alumina and the oxygen atom in the adsorbate reach a certain distance.

The RDF curves of MeOH and DMC from pure solutions and azeotropic mixtures are shown in Figure 9. For all cases, a strong and sharp peak within 3.5 Å was observed, which indicates that those molecules can be strongly adsorbed on the α-Al_2O_3 (0 0 1) surface by forming chemical bonds.[44] The

https://doi.org/10.1021/acsomega.4c10016
ACS Omega 2025, 10, 4026−4036

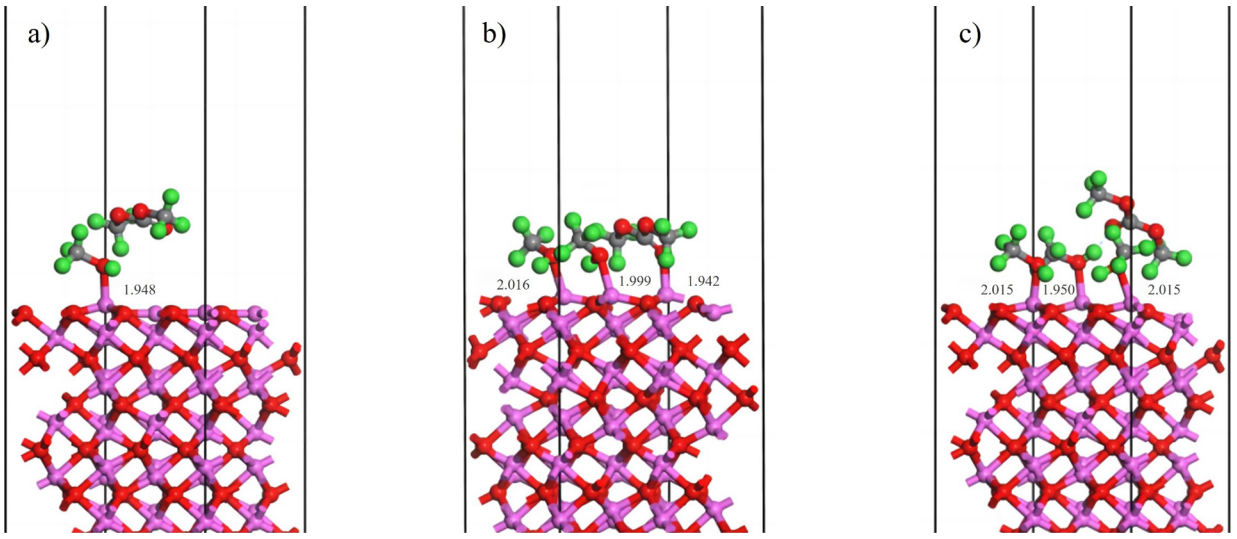

Figure 11. Adsorption of DMC on the surface preadsorbed with (a) 1 MeOH, (b) 2 MeOH, and (c) 3 MeOH.

chemical bonds less than 3.5 Å were considered O−Al bonds.[29,45] In particular, α-Al_2O_3 (0 0 1) has the highest adsorption capacity for azeotropic MeOH. In contrast, the first peak of azeotropic DMC was insignificant showing relatively weak interactions between azeotropic DMC and active sites, while a strong peak beyond 3.5 Å was formed mainly by Coulomb interactions and van der Waals interactions.[46] Previous studies have shown that a chemical bond is formed between the carbonyl oxygen from DMC and the Al_{top} sites when there is no MeOH.[29] However, in the presence of MeOH, it is hard for DMC to interact with Al sites directly. In that case, azeotropic DMC is more likely to bond with adsorbed MeOH forming a multilayer adsorption configuration. As a result, the interaction mechanisms are different for azeotropic and pure DMC molecules.

Our previous study has shown that there is a competition between MeOH and DMC with MeOH molecules being preferentially adsorbed onto the Al active sites.[29] As a result, the α-Al_2O_3 (0 0 1) surface will be covered with abundant MeOH molecules and some DMC molecules. This also might be one of the reasons to explain the difference in the capacities of MeOH and DMC in the azeotrope. Meanwhile, a chemical bond is always formed between hydroxyl O atoms of MeOH and the Al_{top} sites not only for MeOH molecules but also for azeotropic clusters containing MeOH.[29] This indicates that the azeotropic DMC has a minor effect on the bonding pattern between the MeOH and surface Al sites. Therefore, the pure MeOH and azeotropic MeOH show a similar adsorption behavior However, from static experiments and MD simulations, we have observed an increased MeOH adsorption capacity and an enhanced binding strength of MeOH with active sites in the presence of DMC, which cannot be reasonably explained at this moment. Hence, the effect of DMC on preadsorbed MeOH is then investigated by DFT.

3.4. DFT Calculations. In this section, the adsorption of MeOH and DMC on the preadsorbed MeOH was explored by using DFT calculations. The optimized configurations of MeOH and DMC on the surface preadsorbed with 1−3 MeOH molecules are shown in Figures 10 and 11. Instead of forming a chemical bond with other available Al sites, the postadsorbed MeOH tends to form a bilayerlike structure with the preadsorbed MeOH molecules, as seen in Figure 10. Such an adsorption configuration became much less stable with the increase in the coverage of preadsorbed MeOH, judging from the adsorption energy listed in Table 3. Due to the unstable multilayer adsorption configuration and the dissociation of MeOH at high coverage,[47] the adsorption capacity of Al_2O_3 for MeOH is relatively low. However, when there are empty Al sites on the surface, the DMC sometimes tends to form an O−Al bond, as seen in Figure 11b. Meanwhile, a hydrogen bond was also formed between DMC and adjacent preadsorbed MeOH. Even under a high coverage of preadsorbed MeOH, the carboxyl O of DMC can still form a hydroxyl bond with the hydroxyl H of MeOH. Therefore, the adsorption of DMC might further immobilize the MeOH onto Al active sites which could reduce the dissociation of preadsorbed MeOH as well as enhance the configuration stability. As a result, an increased MeOH-adsorption capacity on Al_2O_3 can be observed in the presence of DMC. Although the adsorption energy also increased as listed in Table 3, the energy change was small. Thus, the adsorption of DMC could be more favored when compared with the adsorption of MeOH under the same coverage of preadsorbed MeOH. This can also explain the strong peak observed beyond 3.5 Å by MD simulations, indicating the aggregation of DMC above the preadsorbed MeOH molecules.

Table 3. Adsorption Energy of MeOH and DMC on the Al_2O_3 Surface Preadsorbed with MeOH

	preadsorbed MeOH Molecules		
E_{ads} (kJ/mol)	1 MeOH	2 MeOH	3 MeOH
MeOH	−159.522	−129.193	−31.232
DMC	−207.895	−198.371	−145.251

Based on the differential charge density and electron transfer, the formation of bonds and the charge transfer can be determined and explained more clearly. Thus, the electron density differences of MeOH and DMC on the surface preadsorbed with 1−3 MeOH molecules were investigated and are shown in Figures 12 and 13, with an isosurface of 0.02 au. Yellow represents charge accumulation, while blue represents charge depletion. From Figure 12b,c, it can be seen that it was difficult for the MeOH to approach the active sites once some

https://doi.org/10.1021/acsomega.4c10016
ACS Omega 2025, 10, 4026−4036

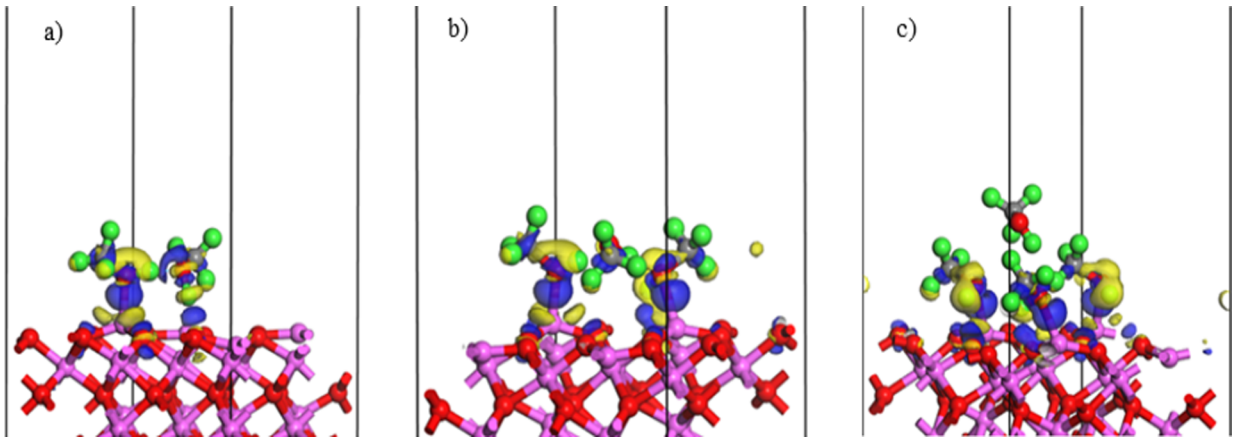

Figure 12. Electron density difference of the adsorption of MeOH on the surface preadsorbed with (a) 1 MeOH, (b) 2 MeOH, and (c) 3 MeOH.

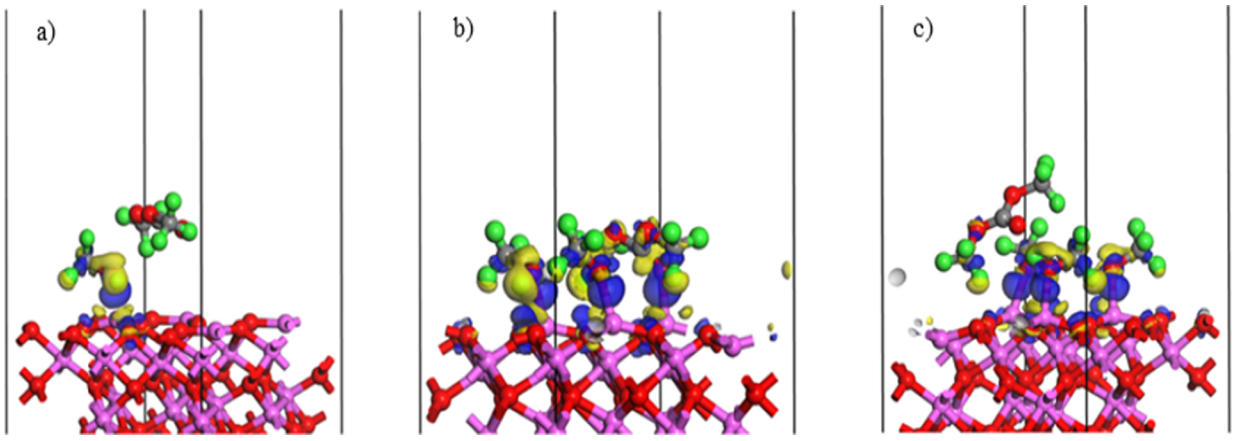

Figure 13. Electron density difference of the adsorption of DMC on the surface preadsorbed with (a) 1 MeOH, (b) 2 MeOH, and (c) 3 MeOH.

MeOH molecules had already existed on the surface. The postadsorbed MeOH barely interacted with the preadsorbed molecules with no electron transfer. From Figure 13b,c, there were overlapping electron clouds between the postadsorbed DMC and the Al site as well as the preadsorbed MeOH, indicating the formation of chemical bonds.

The charge transfer values are listed in Table 4 which can reflect the interaction strength between the adsorbate and the solid surface. It can be seen from Table 4 that the electrons are generally transferred from adsorbates to the α-Al_2O_3 (0 0 1) surface, which is consistent with the electron density difference results. For the adsorption of MeOH and DMC on the surface preadsorbed with 3 MeOH molecules, the cluster transferred 0.53 |e| and 0.68 |e| to the solid surface, respectively. Meanwhile, more electrons transferred from preadsorbed MeOH molecules to the surface. It suggests that the interaction forces between preadsorbed MeOH and active sites in the presence of DMC are greater. In other words, DMC molecules would be preferentially adsorbed on the MeOH layer.

Table 4. Charge Transfer of the Adsorption of MeOH and DMC on the Surface Preadsorbed with MeOH Molecules

preadsorbed molecule	postadsorbed molecule	charge transferred |e|		
		clusters	preadsorption	postadsorption
1 MeOH	MeOH	0.20	0.12	0.08
2 MeOH		0.46	0.37	0.09
3 MeOH		0.53	0.50	0.03
1 MeOH	DMC	0.28	0.27	0.01
2 MeOH		0.59	0.35	0.24
3 MeOH		0.68	0.62	0.06

4. CONCLUSIONS

In this study, the adsorption mechanism of MeOH-DMC onto α-Al_2O_3 as well as the difference between pure and azeotropic components was investigated by conducting experiments and molecular simulations. Static experiment results indicate that α-Al_2O_3 has shown certain adsorption capacities for MeOH and DMC in both pure and azeotropic solutions. The order of the adsorption capacities obtained by the static experiments was: azeotropic MeOH > pure DMC > pure MeOH > azeotropic DMC. Although DMC enhanced the adsorption capacity of MeOH in the azeotrope, no big difference in the mass transfer rate existed between pure and azeotropic MeOH, indicating that DMC contained in the azeotrope will not affect the mass transfer of MeOH from the bulk liquid to the surface sites. However, the MeOH in the azeotrope significantly decreased the adsorption capacity of DMC while altering the adsorption mechanism at the same time. Molecular simulation results indicate that a multilayer adsorption conformation was formed on the α-Al_2O_3 (0 0 1) surface for MeOH-DMC, and most Al sites were occupied by MeOH molecules. Under the MeOH preadsorption condition, the adsorption of DMC can further reduce the dissociation of preadsorbed MeOH by

https://doi.org/10.1021/acsomega.4c10016
ACS Omega 2025, 10, 4026−4036

forming a hydrogen bond, leading to the aggregation of DMC outside the MeOH preadsorption layer.

■ ASSOCIATED CONTENT

Data Availability Statement

All data generated or analyzed during this study are included in this published article.

■ AUTHOR INFORMATION

Corresponding Author

Xueni Sun − *Jiangsu Key Laboratory of Advanced Catalytic Materials and Technology, School of Petrochemical Engineering, Changzhou University, Changzhou 213164, China*; orcid.org/0000-0001-9621-1088; Email: shellysun0110@cczu.edu.cn

Authors

Qiang Fu − *Jiangsu Key Laboratory of Advanced Catalytic Materials and Technology, School of Petrochemical Engineering, Changzhou University, Changzhou 213164, China*

Lidong Li − *Jiangsu Key Laboratory of Advanced Catalytic Materials and Technology, School of Petrochemical Engineering, Changzhou University, Changzhou 213164, China*

Chunxiang Huang − *Jiangsu Key Laboratory of Advanced Catalytic Materials and Technology, School of Petrochemical Engineering, Changzhou University, Changzhou 213164, China*

Jun Wang − *Jiangsu Key Laboratory of Advanced Catalytic Materials and Technology, School of Petrochemical Engineering, Changzhou University, Changzhou 213164, China*; orcid.org/0000-0002-4348-9235

Hui Shao − *Jiangsu Key Laboratory of Advanced Catalytic Materials and Technology, School of Petrochemical Engineering, Changzhou University, Changzhou 213164, China*

Complete contact information is available at: https://pubs.acs.org/10.1021/acsomega.4c10016

Author Contributions

X.S.: Methodology, investigation, data curation, and writing-original draft. Q.F.: Methodology, software, investigation, analysis, and data curation. L.L.: Software, investigation, and data curation. C.H.: Investigation. J.W.: Investigation and validation. H.S.: Methodology, data curation, writing-review, and editing.

Notes

The authors declare no competing financial interest.

■ ACKNOWLEDGMENTS

This work received no financial support. We like to thank the High-Performance Computing Center of Changzhou University for their help with molecular simulations.

■ REFERENCES

(1) Fiorani, G.; Perosa, A.; Selva, M. Dimethyl carbonate: a versatile reagent for a sustainable valorization of renewables[J]. *Green Chem.* **2018**, *20*, 288−322.

(2) Esan, A. O.; Adeyemi, A. D.; Ganesan, S. A review on the recent application of dimethyl carbonate in sustainable biodiesel production-[J]. *Journal of Cleaner Production* **2020**, *257*, No. 120561.

(3) Westbrook, C. K.; Pitz, W. J.; Curran, H. J. Chemical kinetic modeling study of the effects of oxygenated hydrocarbons on soot emissions from diesel engines[J]. *J. Phys. Chem. A* **2006**, *110*, 6912−6922.

(4) Fan, C.; Guan, Z.; Wei, J.; et al. An assessment of soot chemical property from a modern diesel engine fueled with dimethyl carbonate-diesel blends[J]. *Fuel* **2022**, *309*, No. 122220.

(5) Xie, J.; Lu, Y. C. A retrospective on lithium-ion batteries. *Nat. Commun.* **2020**, *11*, 2499.

(6) Shi, D.; Heyte, S.; Capron, M.; et al. Catalytic processes for the direct synthesis of dimethyl carbonate from CO_2 and methanol: a review[J]. *Green Chem.* **2022**, *24*, 1067−1089.

(7) Kontou, V.; Grimekis, D.; Braimakis, K.; et al. Techno-economic assessment of dimethyl carbonate production based on carbon capture and utilization and power-to-fuel technology[J]. *Renewable and Sustainable Energy Reviews* **2022**, *157*, No. 112006.

(8) Huang, H.; Samsun, R. C.; Peters, R.; et al. Greener production of dimethyl carbonate by the power-to-fuel concept: a comparative techno-economic analysis[J]. *Geen Chemistry* **2021**, *23*, 1734−1747.

(9) Deng, Z.; Li, W.; Lin, H.; et al. Research progress of catalysts for synthesis of dimethyl carbonate via direct oxidative carbonylation of methanol. *Fine Chemicals* **2022**, *39* (11), 2196−2214.

(10) An, R.; Chen, S.; Li, H.; et al. Energy-saving reactive pressure-swing distillation process for separation of methanol-dimethyl carbonate azeotrope via reacting with propylene oxide[J]. *Sep. Purif. Technol.* **2022**, *292*, No. 120889.

(11) Li, K.; Cheng, H.; Li, X.; et al. Molecular mechanism-based extractant screening and process design for the separation of methanol/dimethyl carbonate azeotrope[J]. *Sep. Purif. Technol.* **2024**, *333*, No. 125916.

(12) Li, H.; Huang, Y.; Dou, W.; et al. Superwetting membrane-based strategy for highly efficient separation of dimethyl carbonate and methanol. *Sep. Purif. Technol.* **2021**, *341*, No. 126877.

(13) Vopicka, O.; Radotinsky, D.; Friess, K. Sorption of vapour mixtures of methanol and dimethyl carbonate in PDMS: experimental study[J]. *Eur. Polym. J.* **2015**, *73*, 480−486.

(14) Wei, H. M.; Wang, F.; Zhang, J. L.; et al. Design and control of dimethyl carbonate-methanol separation via pressure-swing distillation[J]. *Ind. Eng. Chem. Res.* **2013**, *52* (33), 11463−11478.

(15) Lin, Z.; Tian, W.; An, W. Separation of dimethyl carbonate/methanol via heat pump assisted pressure swing distillation process and system simulation optimization. *Chem. Ind. Eng. Prog.* **2022**, *41* (11), 5722−5730.

(16) Wang, S.; Yu, C.; Huang, H. Plant-wide design and control of DMC synthesis process via reactive distillation and thermally coupled extractive distillation[J]. *Comput. Chem. Eng.* **2010**, *34*, 361−373.

(17) Wang, Y.; Zhang, Z.; Gao, Y.; et al. Extractive distillation separation process of DMC-methanol-water ternary mixture. *Chem. Ind. Eng. Prog.* **2021**, *40* (8), 4196−4204.

(18) Polotskaya, G.; Tian, N.; Faykov, I.; et al. Novel design of co-poly(hydrazide imide) and its complex with Cu(I) for membrane separation of methanol/dimethyl carbonate mixture[J]. *Membranes* **2023**, *13*, 160.

(19) Mahdi, T.; Ahmad, A.; Nasef, M. M.; et al. State-of-the-art technologies for separation of azeotropic mixtures[J]. *Separation & Purification Reviews* **2015**, *44* (4), 308−330.

(20) Cavalcante, C. L. Industrial adsorption separation processes: Fundamentals, modeling and applications. *Latin Am. Appl. Res.* **2000**, *30* (4), 357−364.

(21) Spencer, M. S. Carbonate production: US, 4582645 (Apr 15, 1986).

(22) Fan, W. W.; Wang, X. J.; Li, W.; et al. Adsorption separation of dimethyl carbonate and methanol azeotrope. *Chem. Eng.* **2010**, *38* (1), 10−13.

(23) Karimi, S.; Yaraka, M. T.; Karri, R. R. A comprehensive review of the adsorption mechanisms and factors influencing the adsorption process from the perspective of bioethanol dehydration. *Renewable Sustainable Energy Rev.* **2019**, *107*, 535−553.

(24) Sun, X.; Tian, L.; Chen, S.; et al. Optimization of aluminium oxide/acid-treated palygorskite by response surface methodology and its application in adsorptive separation of the methanol-dimethyl carbonate azeotrope. *ChemistrySelect* **2023**, *8* (15), No. e202204423.
(25) Sun, X.; Chen, S.; Xie, H.; et al. Adsorption separation performance of methanol-dimethyl carbonate by CTAB/Al_2O_3/ATP adsorbent. *Acta Pet. Sin.* **2021**, *37* (5), 994−1001.
(26) Wang, Y.; Wang, B.; Li, W. Theoretical investigation on the adsorption of nitroglycerin on the α-Al_2O_3(0001) and γ-Al_2O_3(110) surfaces. *Chem. J. Chin. Univ.* **2017**, *38* (8), 1383−1389.
(27) Yang, C.; Li, Y. R.; Yan, Q. L.; et al. Effects of atomic defects of α-Al_2O_3 (0001) on ZnO adsorption. *Acta Phys. Sin.* **2005**, *54* (5), 2364−2368.
(28) Hao, Y.; Niu, S.; Li, Y.; et al. Molecular simulation of hydroxyl activated by methanol adsorption on Zn-modified Sr/γ-Al_2O_3 surface. *Trans. Chin. Soc. Agric. Eng.* **2022**, *38* (9), 253−260.
(29) Sun, X.; Li, A.; Tan, H.; et al. Experimental investigation and molecular simulations of adsorption of MeOH-DMC azeotrope onto α-Al_2O_3 (0 0 1) surface. *Mol. Phys.* **2023**, *122* (11), No. e2290208.
(30) Darriba, G. N.; Faccio, R.; Rentería, M. First-principles study of Cd impurities localized at and near the (0 0 1) α-Al_2O_3 surface[J]. *Comput. Mater. Sci.* **2015**, *107*, 15−23.
(31) He, Y. J.; Ma, B. Molecular dynamics analysis on bending mechanical behavior of alumina nanowires at different loading rates. *Trans. Nonferrous Met. Soc. China* **2022**, *32* (11), 3687−3698.
(32) Dixit, M. K.; Tembe, B. L. Potentials of mean force of sodium chloride ion pair in dimethyl sulfoxide−methanol mixtures[J]. *J. Mol. Liq.* **2013**, *178*, 78−83.
(33) Durbin, T. D.; Karavalakis, G.; Johnson, K. C. *Evaluating the Viability of Dimethyl Carbonate as an Alternative Fuel for the Transportation Sector*; NCST: 2017.
(34) Aminabhavi, T. M.; Banerjee, K. Density, viscosity, refractive index, and speed of sound in binary mixtures of dimethyl carbonate with methanol, chloroform, carbon tetrachloride, cyclohexane, and dichloromethane in the temperature interval (298.15−308.15) K[J]. *Journal of Chemical & Engineering Data* **1998**, *43* (6), 1096−1101.
(35) Wang, J.; Guo, X. Adsorption kinetic models: physical meanings, applications, and solving methods[J]. *Journal of Hazardous Materials* **2020**, *390*, No. 122156.
(36) Guo, X.; Wang, J. A general kinetic model for adsorption: theoretical analysis and modeling[J]. *J. Mol. Liq.* **2019**, *288*, No. 111100.
(37) Stoyanov, E. S.; Stoyanova, I. V.; Reed, C. A. IR spectroscopic properties of H $(MeOH)_{n+}$ clusters in the liquid phase: Evidence for a proton wire[J]. Chemistry−A. *European Journal* **2008**, *14* (12), 3596−3604.
(38) Myerson, A. S.; Jang, S. M. Comparison of binding energy and metastable zone width for adipic acid with various additives[J]. *J. Cryst. Growth* **1995**, *156* (4), 459−466.
(39) Zheng, R.; Ren, Z.; Gao, H.; et al. Effects of crystal chemistry on sodium oleate adsorption on fluorite surface investigated by molecular dynamics simulation[J]. *Minerals Engineering* **2018**, *124*, 77−85.
(40) Blackberg, L.; Metsanurk, E.; Tamm, A.; et al. Molecular dynamics study for xenon on an amorphous Al_2O_3 surface[J]. *Nuclear Instruments and Methods in Physics Research A: Accelerators, Spectrometers, Detectors and Associated Equipment* **2014**, *759*, 10−15.
(41) Hu, S. Q.; Guo, A. L.; Yan, Y. G.; et al. Computer simulation of diffusion of corrosive particle in corrosion inhibitor membrane[J]. *Computational and Theoretical Chemistry* **2011**, *964*, 176−181.
(42) Zhang, J.; Clennell, M. B.; Dewhurst, D. N.; et al. Combined Monte Carlo and molecular dynamics simulation of methane adsorption on dry and moist coal[J]. *Fuel* **2014**, *122*, 186−197.
(43) Li, B.; Guo, J.; Liu, S.; et al. Molecular insight into the mechanism of benzene ring in monionic surfactants on low-rank coal floatability[J]. *J. Mol. Liq.* **2020**, *302*, No. 112563.
(44) Xu, X. T.; Xu, H. W.; Cui, Y. F.; et al. Molecular dynamics study of three amino acids as corrosion inhibitor for copper in hydrochloric acid solution. *J. Mol. Model.* **2022**, *28*, 55.
(45) Keyvanloo, Z.; Pour, A. N.; Moosavi, F.; et al. Molecular dynamic simulation studies of adsorption and diffusion behaviors of methanol and ethanol through ZSM-5 zeolite. *J. Mol. Graph. Model.* **2022**, *110*, No. 108048.
(46) Zeng, J.; Zhang, J.; Gong, X. Molecular dynamics simulation of interaction between benzotriazoles and cuprous oxide crystal[J]. *Computational and Theoretical Chemistry* **2011**, *963*, 110−114.
(47) Tilocca, A.; Selloni, A. Methanol adsorption and reactivity on clean and hydroxylated anatase(1 0 1) surfaces[J]. *J. Phys. Chem. B* **2004**, *108*, 19314−19319.

https://doi.org/10.1021/acsomega.4c10016
ACS Omega 2025, 10, 4026−4036